Hierarchical ZSM-5 Zeolites in Shape-Selective Xylene Isomerization: Role of Mesoporosity and Acid Site Speciation

ARTICLE *in* CHEMISTRY - A EUROPEAN JOURNAL · JUNE 2010

Impact Factor: 5.73 · DOI: 10.1002/chem.200903426 · Source: PubMed

7 AUTHORS, INCLUDING:

Jean-Pierre Gilson
ENSICAEN (Caen)
119 PUBLICATIONS **2,317** CITATIONS
SEE PROFILE

Aurélie Vicente
Université de Caen Normandie
28 PUBLICATIONS **374** CITATIONS
SEE PROFILE

Javier Pérez-Ramírez
ETH Zurich
308 PUBLICATIONS **8,471** CITATIONS
SEE PROFILE

CHEMISTRY
A EUROPEAN JOURNAL

DOI: 10.1002/chem.200903426

Hierarchical ZSM-5 Zeolites in Shape-Selective Xylene Isomerization: Role of Mesoporosity and Acid Site Speciation

Christian Fernandez,*[a] Irina Stan,[a] Jean-Pierre Gilson,[a] Karine Thomas,[a] Aurélie Vicente,[a] Adriana Bonilla,[b] and Javier Pérez-Ramírez*[b, c]

Abstract: The isomerization of *o*-xylene, a prototypical example of shape-selective catalysis by zeolites, was investigated on hierarchical porous ZSM-5. Extensive intracrystalline mesoporosity in ZSM-5 was introduced by controlled silicon leaching with NaOH. In addition to the development of secondary porosity, the treatment also induced substantial aluminum redistribution, increasing the density of Lewis acid sites located at the external surface of the crystals. However, the strength of the remaining Brønsted sites was not changed. The mesoporous zeolite displayed a higher *o*-xylene conversion than its parent, owing to the reduced diffusion limitations. However, the selectivity to *p*-xylene decreased, and fast deactivation due to coking occurred. This is mainly due to the deleterious effect of acidity at the substantially increased external surface and near the pore mouths. A consecutive mild HCl washing of the hierarchical zeolite proved effective to increase the *p*-xylene selectivity and reduce the deactivation rate. The HCl-washed hierarchical ZSM-5 displayed an approximately twofold increase in *p*-xylene yield compared to the purely microporous zeolite. The reaction was followed by operando infrared spectroscopy to simultaneously monitor the catalytic performance and the buildup of carbonaceous deposits on the surface. Our results show that the interplay between activity, selectivity, and stability in modified zeolites can be optimized by relatively simple post-synthesis treatments, such as base leaching (introduction of mesoporosity) and acid washing (surface acidity modification).

Keywords: acidity · catalyst design · deactivation · IR spectroscopy · zeolites

Introduction

The history of zeolite catalysis is firmly rooted in the oil and petrochemical industry.[1] Over the years, a series of synthetic zeolites (X and Y, MOR, ZSM-5, beta, MCM-22, ZSM-22, ZSM-23, etc.) have been discovered and subsequently applied with considerable success in important oil-refining and petrochemical processes. Parallel to this wave of innovation in industrial catalysis, the scientific foundations of their unique selectivity were laid down by industrial and academic scientists.[2] It is remarkable that, although so many zeolite frameworks exist,[3] only a handful is responsible for their major industrial applications. The explanation lies, in part, in the extraordinary creativity of scientists and engineers to design post-synthesis treatments for a few zeolites to fine-tune their catalytic properties to many reactions and reactors.

Modern catalyst design is a challenge of optimization, because activity and selectivity often have contradictory requirements. For instance, when shape-selective zeolite catalysis is based on diffusion constraints on either reactants or products, selectivity is enhanced by working with large zeolite crystals.[4] The use of such crystals results, however, in lower activity due to suboptimal utilization of all the active sites present. Smaller crystals, on the other hand, could display an increased activity but a lower selectivity. Hierarchical porous zeolites, that is, zeolites containing their native micropores along with an auxiliary network of mesopores have attracted much attention due to their potential in catal-

[a] Prof. C. Fernandez, Dr. I. Stan, Prof. J.-P. Gilson, Dr. K. Thomas, Dr. A. Vicente
Laboratoire Catalyse et Spectrochimie, ENSICAEN, Université de Caen, CNRS
6 Bd du Maréchal Juin, 14050 Caen (France)
Fax: (+33) 231-45-2822
E-mail: christian.fernandez@ensicaen.fr

[b] Dr. A. Bonilla, Prof. J. Pérez-Ramírez
Institute of Chemical Research of Catalonia (ICIQ)
Avinguda dels Països Catalans 16, 43007 Tarragona (Spain)

[c] Prof. J. Pérez-Ramírez
Institute for Chemical and Bioengineering
Department of Chemistry and Applied Biosciences
ETH Zurich, HCI E125, 8093 Zurich (Switzerland)
E-mail: jpr@chem.ethz.ch

Supporting information for this article is available on the WWW under http://dx.doi.org/10.1002/chem.200903426.

ysis.[5] The benefits of hierarchical zeolites have been reported in a wide range of catalyzed reactions, such as aromatization,[6] isomerization,[6,7] oligomerization,[8] esterification,[7] alkylation,[9] acylation,[10] cracking,[7] pyrolysis,[11] methanol conversion,[12] and selective oxidation.[13] In particular, the controlled extraction of framework silicon in existing zeolites, referred to as desilication or base leaching, is a top-down approach to prepare hierarchical porous zeolites.[14] It holds much promise due to its applicability as a post-synthesis treatment of commercially available zeolites.

A key question in the design of superior shape-selective hierarchical zeolite catalysts is how to further fine-tune the acidity located in the native micropores and the newly created mesopores, to optimize catalytic performance. For instance, the increasing role of the external and mesoporous surface cannot be neglected, because it is the locus of many reactions.[15,16] Some of these lack the shape-selective control found in the micropores (e.g., coking), whereas others are claimed to be based on properties specific to the external surface (e.g., liquid-phase cumene synthesis on MCM-22 in which a "nest effect" could explain its outstanding catalytic performance).[4] The exact nature of this selectivity is often subject to much debate, as it is not always straightforward to distinguish it from more classical shape-selectivity effects (reactants, products, and transition state) occurring inside the micropores. In the case of hierarchical ZSM-5 prepared by a bottom-up approach, Ryoo et al.[17] reported the activity of the mesoporous walls in the acid-catalyzed conversion of bulky molecules and the effect of their selective dealumination on catalytic activity. Acid treatment of zeolites can affect their acidity and texture in many ways. It can either remove some extra-framework Al under mild conditions or extensively dealuminate the zeolitic framework and create mesoporosity under more severe conditions.[16] Previous work[18] showed that mesopore formation and acidity modification in ZSM-5 zeolites can be decoupled by sequential desilication by NaOH and steam dealumination; the interesting catalytic consequences of such a two-step treatment in aromatization and isomerization of *n*-hexene were reported recently.[19] These consecutive treatments lead, however, to complex systems in which the various forms of acidity (Brønsted, Lewis, enhanced sites)[20] can produce an heterogeneity of active sites, and muddles correlations between acidity and the resulting catalytic activity.

The application of mesoporous zeolites in mixed xylene isomerization has not yet been explored. Mixed xylene isomerization (usually in the presence of ethylbenzene) to produce *p*-xylene, the most desired isomer, is a major industrial application of zeolites.[1,2] It is also a model reaction (feed is either pure *o*- or *m*-xylene) to assess the shape selectivity of microporous materials.[21] An intramolecular mechanism takes place inside the restricted microporosity of zeolites such as ZSM-5 and is responsible for the selective production of *p*-xylene, the isomer with the fastest intracrystalline diffusion.[22] An intermolecular mechanism, leading ultimately to coke, takes place in less restricted environments such as the external surface of the crystals and the mesopores. A precise understanding of all factors involved in this simple test reaction will generate very useful information towards a better understanding of more complex reactions (e.g., methanol to hydrocarbons and coking in general).

The aim of this paper is to highlight the combined effects of two straightforward liquid-phase post-synthesis treatments of ZSM-5, namely, desilication (base leaching) followed by dealumination (mild acid washing), on the conversion of *o*-xylene to *p*-xylene. These two easily upscalable treatments belong to the toolbox for rationally designing zeolytic catalysts. The resulting catalysts were characterized by well-established techniques and by operando infrared (IR) spectroscopy.[23] This method facilitates the simultaneous measurement of the catalytic properties (activity, selectivity, and stability) and the monitoring of the surface of the working catalyst. Particular attention was paid to the time-on-stream variation of the hydroxyl groups (silanols and bridged hydroxyls), the coking, and their relationship by 2D-correlation spectroscopy. The potential of the methodology has already been demonstrated for this reaction, albeit at lower temperatures (473–573 K).[23] This is a first step in the rational design of catalysts by combining industrially feasible, material design techniques with state-of-the-art characterization and testing methods.

Results and Discussion

Influence of post-synthesis treatments: Throughout the manuscript, the samples are denoted as P, H, and HW. P refers to the parent H-ZSM-5 zeolite. Sample H (hierarchical) results from NaOH treatment of sample P followed by ion exchange with NH_4NO_3. Sample HW (hierarchical and washed) is obtained by HCl treatment of sample H. Details can be found in the Experimental Section.

Alkaline treatment: Treatment of ZSM-5 zeolites with Si/Al = 25–50 in aqueous NaOH solutions under the conditions used in this work (0.2 M, 338 K, 30 min) is known to generate extensive intracrystalline mesoporosity in the zeolite by selective extraction of framework silicon.[14,25,26] In this particular sample, the molar Si/Al ratio decreases from 47 in P to 33 in H (Table 1). The amount of dissolved silicon in the filtrate is three orders of magnitude higher than that of aluminum and the development of mesoporosity is clearly observed by gas adsorption. Figure 1 shows that the typical type I N_2 isotherm in the purely microporous sample transforms into a combined I and IV isotherm in the NaOH-treated sample, a known fingerprint of a hierarchical porous system.[5] The mesopore surface area (S_{meso}) increases from 62 to 250 $m^2 g^{-1}$ and the micropore volume (V_{micro}) concomitantly decreases from 0.17 to 0.13 $cm^3 g^{-1}$ (Table 1). In other words, the fourfold increase in S_{meso} implies a reduction of approximately 25% of the original V_{micro}. The hierarchical sample exhibits a mesopore distribution centered at 8 nm (Figure 1, inset). Equivalent conclusions are extracted from high-resolution low-pressure argon adsorption at 87 K. The

Table 1. Characterization of the parent (P) and treated (H, HW) ZSM-5 samples.

Property	Sample P	Sample H	Sample HW
Al content[a] [μmol g^{-1}]	333	456	304
molar ratio (Si/Al)$_{bulk}$[a]	47	33	51
molar ratio (Si/Al)$_{surface}$[b]	32	16	47
Si$_{filtrate}$[a] [ppm]	–	4777	95
Al$_{filtrate}$[a] [ppm]	–	4	156
V_{pore}[c] [cm^3 g^{-1}]	0.27	0.58	0.60
V_{micro}[d] [cm^3 g^{-1}]	0.17	0.13	0.12
S_{meso}[d] [m^2 g^{-1}]	62	250	275
S_{BET}[e] [m^2 g^{-1}]	457	578	573
B$_{py}$[f] [μmol g^{-1}]	314	205	185
L$_{py}$[f] [μmol g^{-1}]	37	208	121
B$_{py}$/Al	0.94	0.45	0.61
L$_{py}$/Al	0.11	0.46	0.40
B$_{lu}$[g] [μmol g^{-1}]	93	219	171
B$_{coll}$[h] [μmol g^{-1}]	9	48	24
ACI$_{py}$[i]	1.05	0.91	1.01
ACI$_{lu}$[i]	0.30	1.07	0.92
ACI$_{coll}$[i]	0.03	0.23	0.13
$\Delta\nu$(OH)[j] [cm^{-1}]	315	315	315
ν(OH)[j] [cm^{-1}]	315	315	315

[a] Measured by ICP-OES. [b] Measured by XPS. [c] Measured by N_2 adsorption, $V_{ads,p/p0}=0.99$. [d] *t*-plot. [e] BET method. [f] Brønsted (B) and Lewis (L) acid sites measured by IR spectroscopy of adsorbed pyridine. [g] Measured by IR spectroscopy of adsorbed lutidine. [h] Measured by IR spectroscopy of adsorbed collidine. [i] ACI (Accessibility Index), determined by using the definition given elsewhere.[24] [j] Measured by IR spectroscopy of adsorbed CO.

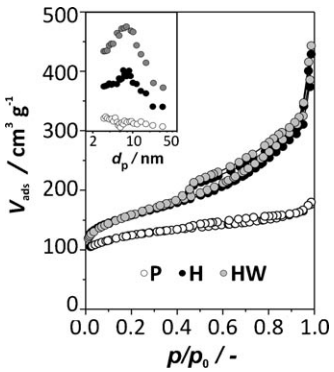

Figure 1. N_2 isotherms at 77 K of the parent (P) and treated (H, HW) ZSM-5 zeolites. The pore size distributions (inset) were determined by application of the BJH model on the adsorption branch of the isotherm. NaOH treatment induces the formation of mesopores centered at 8 nm (sample H). A consecutive treatment of H with HCl does not modify the porosity further (sample HW).

corresponding isotherms are in Figure SI1, in the Supporting Information.

Transmission electron microscopy (Figure 2) highlights the intracrystalline nature of the newly generated mesopores and confirms the size determined from nitrogen adsorption. Despite such drastic porosity changes, the alkaline-treated sample displays the characteristic diffraction pattern of the MFI structure, indicating the preservation of the long-range order in the hierarchical zeolite (Figure SI2 in the Supporting Information). The intensity of the reflections in sample

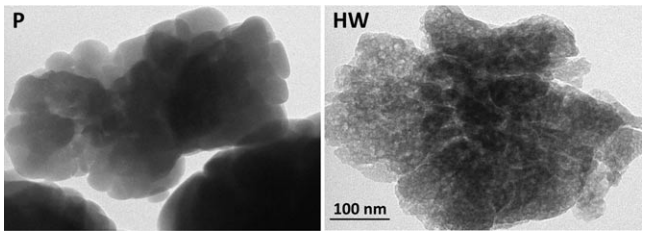

Figure 2. Transmission electron micrographs of the parent (P) and treated (HW) ZSM-5 zeolites. The uniform distribution of intracrystalline mesopores can be visualized in the hierarchical samples. The micrographs of samples H and HW were very similar and, to save space, only one of them is displayed.

H is slightly lower than that in sample P, probably because smaller crystalline domains are formed upon silicon extraction.

In addition to the above-described compositional and porosity modifications, the NaOH treatment induces remarkable acidity changes, which play a crucial role in the catalytic performance of the modified zeolites (vide infra). The infrared spectra of the dehydrated P and H samples (Figure 3)

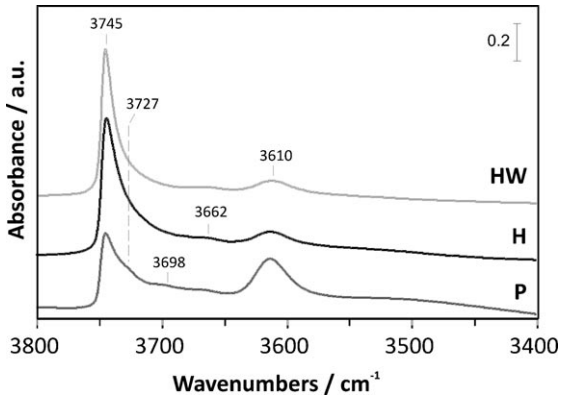

Figure 3. FTIR spectra of the dehydrated parent (P) and treated (H, HW) ZSM-5 zeolites in the hydroxyl vibration region. The spectra were recorded at room temperature.

show various bands that could be attributed to 1) isolated silanols at the external surface of the zeolite (3745 cm^{-1}), 2) perturbed silanols mainly located inside the zeolite crystals (3727 cm^{-1} and 3698 cm^{-1}),[23] 3) Al(OH) groups corresponding to extra-framework species (3662 cm^{-1}), 4) Al(OH)Si groups corresponding to strongly acidic Brønsted sites (3610 cm^{-1}), and 5) a broad band corresponding to silanols interacting through hydrogen bonding (3500 cm^{-1}).[27] The intensity of the silanol band at 3745 cm^{-1} increases in the hierarchical zeolite, in agreement with its increased external surface area. The 3610 cm^{-1} band decreases upon base leaching, suggesting that this treatment also changes the density of strong acid sites significantly.

Infrared spectroscopy of adsorbed pyridine (Table 1) indicates that the parent sample contains mainly Brønsted acidity; only 10% of the total acid sites, (B$_{py}$+L$_{py}$)/Al, are Lewis

acidic. However, the relative amount of Lewis sites in the mesoporous zeolite H increases by a factor of four relative to the parent zeolite P. In the former sample, the distribution of Brønsted and Lewis acidity is practically 50:50, clearly pointing to a transformation of Brønsted sites into Lewis sites. The density of Brønsted acid sites per gram of zeolite decreases by 35% in sample H relative to sample P. However, the strength of the remaining Brønsted sites (3610 cm^{-1}), measured by infrared spectroscopy of adsorbed CO, does not change between P and H, as indicated by the $\Delta\nu$(OH) value in Table 1 (see also Figure SI3 in the Supporting Information). This feature is in good agreement with spectroscopic studies on desilicated ZSM-5 by Holm et al.[27] IR spectra in the ν(CO) region of sample H also show the appearance of a band at 2230 cm^{-1} upon CO adsorption, corresponding to strong Lewis sites (Figure SI3 in the Supporting Information). This band is hardly detected in the parent zeolite, in agreement with the much lower density of Lewis acid sites. Infrared spectroscopy of bulkier adsorbed alkylpyridines reveals that after the alkaline treatment, all Brønsted sites are accessible to 2,6-dimethylpyridine (lutidine). The "accessibility index"[24] of lutidine (ACI_{lu}) is thus 1 for zeolite H, whereas it is only 0.3 for zeolite P. Moreover, about 23% of the Brønsted sites are probed by 2,4,6-trimethylpyridine (collidine) ($ACI_{coll} \approx 0.23$) in zeolite H compared to only 3% in zeolite P.

The extraction of some tetrahedral Al to extra-framework positions during NaOH treatment is confirmed by ^{27}Al MAS NMR spectroscopy. Sample P exhibits a single peak at about 55 ppm corresponding to framework Al in tetrahedral coordination, while sample H contains an additional peak centered around 0 ppm due to extra-framework Al in octahedral coordination (Figure 4).

The generation of Lewis sites upon desilication can be explained by considering the mechanism of this post-synthesis treatment. The OH^- groups in the sodium hydroxide solution first attack defects on the external surface of the zeolite (low-coordinate silicon) and extract solid fragments, gradually dissolving to monomeric species in the basic medium.[26,28] Aluminum species then reprecipitate on the zeolite external surface. As shown in Table 1 (third row), the surface composition of the zeolite measured by XPS indicates that the Si/Al ratio in sample H (16) is half of the value measured in sample P (32), highlighting an Al enrichment of the surface in the hierarchical zeolite prepared by desilication in NaOH. However, this process is not purely a re-alumination,[29] because Al^{3+} is not fully reinserted in the ZSM-5 framework. Indeed, both ^{27}Al MAS NMR and IR spectroscopy of adsorbed pyridine indicate that a substantial fraction of the extracted aluminum gives rise to Lewis acidity.

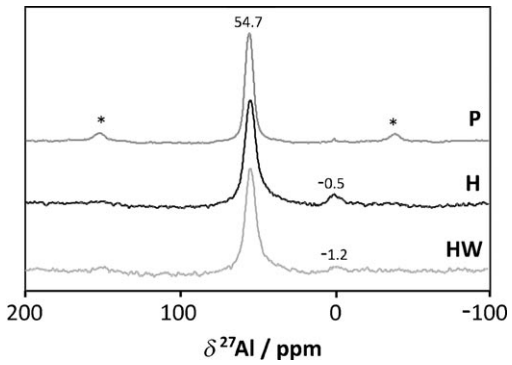

Figure 4. ^{27}Al MAS NMR spectra of the parent (P) and treated (H, HW) ZSM-5 zeolites. The main resonance around 55 ppm corresponds to framework Al, while the resonance around 0 ppm corresponds to extra-framework Al. The asterisks indicate the position of the spinning sidebands.

Acid treatment: The alkaline-treated sample in aqueous HCl (0.1 M, 343 K, 6 h) was mildly washed to modify the surface acidity of the hierarchical zeolite, that is, to decrease the amount of acid sites on the crystals' external surface. As will be shown in the next section, Lewis and Brønsted acidity close to the pore mouths are detrimental to the *para* selectivity and stability of *o*-xylene isomerization. The Si/Al ratio of sample HW increases relative to that of sample H (from 33 to 51), indicating the high effectiveness of the HCl treatment in removing Al. However, the same acid washing conditions applied to the parent zeolite do not alter its Si/Al ratio. Thus, aluminum in the hierarchical zeolite, probably in nonframework positions, is more susceptible to dissolve than in its parent. The lower stability of the hierarchical porous zeolite in acids is therefore due to the redistribution of aluminum species caused by the alkaline treatment. The action of the mild HCl treatment is quite likely mostly restricted to the external surface of the samples. Indeed, the porosity (N_2 adsorption at 77 K, Figure 1 and Table 1 as well as argon adsorption at 87 K, Figure SI1 in the Supporting Information), morphology (TEM, Figure 2), and crystallinity (XRD, Figure SI2 in the Supporting Information) in H and HW are almost identical.

Upon HCl washing (HW) of the desilicated sample (H), the distribution of the acid sites changes. According to IR spectroscopy of adsorbed pyridine, on a weight of zeolite basis, 42% of Lewis acid sites and 10% of the Brønsted acid sites present in sample H are removed. On a molar aluminum basis, sample HW loses 13% of Lewis sites and gains 35% of Brønsted sites relative to preceding sample H. Most of the Brønsted sites detected by pyridine are also accessible to lutidine ($ACI_{lu} = 0.92$) in sample HW. Interestingly, collidine has access to only 13% of the Brønsted sites of the HW sample, whereas it probes up to 23% in the H sample. This highlights that strong acid sites are mainly removed from the external surface. XPS analysis confirms this observation and points also to a significantly enhanced surface Si/Al ratio of 47 in sample HW compared to the value of 16 in sample H (Table 1). In fact, the surface of the acid-washed hierarchical ZSM-5 is more siliceous than that of the parent P. Moreover, the IR spectra of the ν(OH) region (Figure 3) show that the silanol band is slightly narrower for the acid-washed sample, HW, due to a reduced intensity of the internal silanol band (3727 cm^{-1}) compared to that of

both P and H zeolites. Therefore, we conclude that HCl washing mainly removes Lewis acid sites, in extra-framework positions, located at the external surface of the mesopores. This is confirmed by ^{27}Al MAS NMR, showing for HW a decrease of the 0 ppm peak, associated with extra-framework aluminum (Figure 4). Moreover, the increased number of Brønsted sites and the decrease of internal silanols could indicate some reinsertion of aluminum in framework positions. Despite this substantial acidity modification, the strength of the Brønsted sites in HW, measured by infrared spectroscopy of adsorbed CO, is very similar to that in H and P (Table 1). As for sample H, the IR spectra of sample HW in the ν(CO) region shows a band at 2230 cm^{-1}, corresponding to strong Lewis sites, as well as a new band at 2188 cm^{-1}, due to Lewis sites with weaker acidity (Figure SI3 in the Supporting Information).

Thus, while the NaOH treatment alters both the porosity and acid site distribution of the parent zeolite, the subsequent mild HCl washing fine-tunes the acidic properties of the hierarchical zeolite without affecting its porous properties.

Catalytic performance and state of the working catalyst: All catalytic results were acquired on the operando IR set-up described elsewhere.[14] Conversion, selectivity, and stability were measured by GC analysis of the reaction products at 673 K (weight hourly space velocity (WHSV) = 4.1–4.9 h^{-1}). The surface of the working catalysts was monitored simultaneously by IR spectroscopy.

Product analysis indicates the presence of the three xylene isomers; other (disproportionation) products are present but in negligible amounts. The *o*-xylene conversion on the parent zeolite is systematically lower than on the mesoporous zeolites over the whole duration of the run (Figure SI4 in the Supporting Information) While the alkaline-treated zeolite H deactivates faster than its parent P, a consecutive acid washing (HW) leads to a more stable catalyst (Figure 5). The more siliceous nature of the surface of the acid-washed hierarchical ZSM-5 compared to the parent

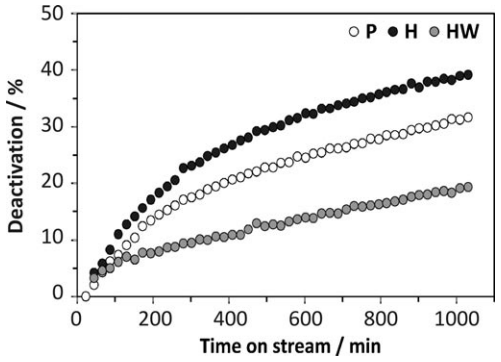

Figure 5. Deactivation of the ZSM-5 catalysts as a function of time on stream. The deactivation is defined as $(X_0-X)/X_0$, where X_0 is the initial *o*-xylene conversion and X is the *o*-xylene conversion at time t. The hierarchical sample (H) displays the fastest deactivation rate; it is considerably reduced upon subsequent acid washing (HW).

ZSM-5 represents a distinctive advantage in the stability of the zeolite in *o*-xylene isomerization. The selectivity to *p*-xylene is the highest on the parent ZSM-5 due to (product) shape selectivity (Figure 6). The creation of mesopores by

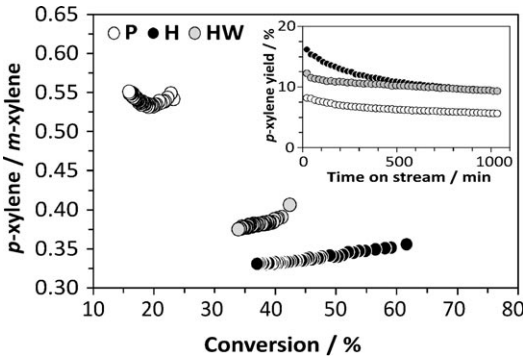

Figure 6. *p*-Xylene selectivity versus *o*-xylene conversion at 623 K over the ZSM-5 catalysts. The treatment of the parent sample (P) by NaOH (H) decreases the *p*-xylene selectivity. Subsequent HCl washing (HW) increases the *p*-xylene selectivity. The inset shows the *p*-xylene yield versus time on stream, always higher for the modified zeolites (H, HW) than for the parent (P).

alkaline treatment (sample H) results in a markedly decreased selectivity to *p*-xylene. However, the acid-washed hierarchical zeolite (HW) increases *p*-xylene selectivity by 18% (measured at 40% *o*-xylene conversion) relative to the H zeolite; the *p*-xylene yield after 17 h on stream is approximately 70% higher for H and HW than for the parent sample (Figure 6, inset). The deactivation rate being slower for HW, it can reasonably be expected that the *p*-xylene yield would ultimately be higher for HW than for H. Since the acidity (Brønsted and Lewis) of the mesoporous surface of sample HW is reduced compared to sample H, the acidic washing of the desilicated zeolite clearly improves the *para* selectivity as the (monomolecular) shape-selective reaction is favored in the internal microporous network. The treatment also improves catalyst stability, because the active sites on the external surface are the loci of unwanted (bimolecular, such as coking) reactions.[30] Thermogravimetric analysis of the used catalysts in air indicates that sample HW contains about half the coke content of sample H, in agreement with lower deactivation rate of the former specimen (Figure 7).

The IR monitoring of the surface during the reaction shows interesting features. Upon *o*-xylene introduction, the intensity of the silanol band at 3730–3737 cm^{-1} decreases for all samples (Figure 8, top). In the difference spectra, the silanol bands display a negative variation (Figure 8, bottom), the largest on sample H. A positive contribution, between 3690 and 3600 cm^{-1}, is likely caused by silanols in interaction with reactants and products. For all samples, the Brønsted sites (3598 cm^{-1}) are only slightly affected by the reaction (no more than a 1–2% decrease in intensity).

In the ν(CH) region (Figure 9, left), two bands at 3030 and 3066 cm^{-1} are characteristic of CH directly linked to

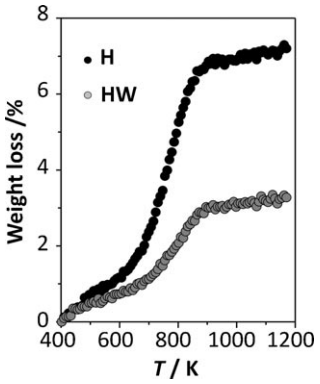

Figure 7. Thermogravimetric analysis of the hierarchical zeolites after catalytic test in *o*-xylene isomerization.

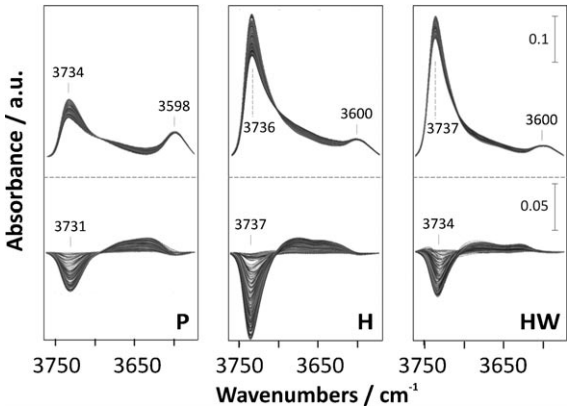

Figure 8. Top: Series of infrared spectra of the ZSM-5 catalysts in the ν(OH) region during 17 h of *o*-xylene isomerization at 623 K. Bottom: Difference spectra relative to the spectra recorded before the onset of reaction.

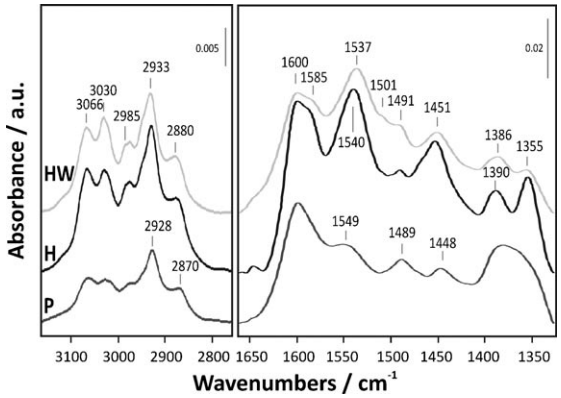

Figure 9. IR spectra recorded after 17 h of *o*-xylene isomerization at 623 K on the parent (P) and treated (H, HW) ZSM-5 catalysts.

aromatic rings, while three bands below 3000 cm^{-1} make up the signature of symmetric and asymmetric stretching of CH in alkyl groups.[31] Their intensities continuously increase during the 17 h of reaction and they likely correspond to aromatic and polyaromatic products (coke) progressively deposited on the zeolite surface. The ratio of the aromatic CH to the alkyl CH intensity is about 20% higher in samples H and HW than in sample P. This indicates that the coke formed could be slightly more aromatic (heavier) on the hierarchical zeolites than in the purely microporous zeolite.

In the aromatic region between 1300 and 1700 cm^{-1}, several bands grow continuously with time on stream (Figure 9, right). Their intensity is highest in sample H, indicating that more coke is deposited on this sample than on samples P and HW. This agrees well with the TGA (thermogravimetric analysis) results in Figure 7. Several authors report a strong correlation between coke formation on the zeolite and the band at 1585 cm^{-1}, due to the ν(C=C) vibration of polycyclic species (graphitic carbon structures).[32] This band is more intense on H and HW than on P, strongly suggesting that the coke formed is more aromatic on the mesoporous zeolites than on the parent sample. The band at 1385 cm^{-1} is generally attributed to CH bending vibrations in alkyl groups.[33] Most of the other bands are characteristic of the ν(C=C) vibrations of aromatic rings, although their unequivocal assignment is quite complex and beyond the scope of this paper.

To better understand the nature of the species present on the catalysts after 17 h of reaction, the catalysts are purged for 3 h under a flow of pure N_2 (Figure 10). Less than 10% of the adsorbed aromatic species are removed under these conditions, that is, 90% remain on the catalyst. In the parent ZSM-5, only the bands at 1355 cm^{-1} and between 1540–1550 cm^{-1} are unaffected upon N_2 flushing. These bands thus correspond to strongly adsorbed aromatic or polyaromatic (coke) molecules. In contrast, the bands appearing in the difference spectra (Figure 10) are typical of light aromatic molecules easily desorbed upon N_2 flushing. Ac-

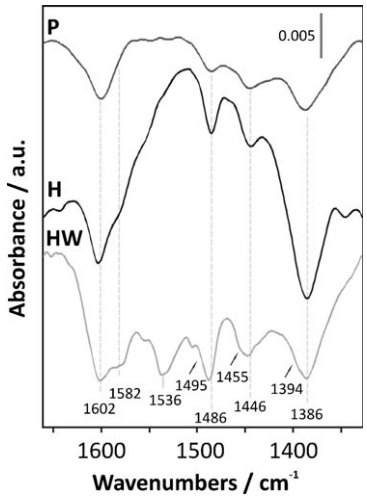

Figure 10. IR difference spectra of the parent (P) and treated (H, HW) ZSM-5 catalysts after 17 h of *o*-xylene reaction at 623 K for 17 h, followed by N_2 flushing at the same temperature for 3 h. The reference was taken as the first spectra in the series, just after the interruption of the *o*-xylene reactant flow.

cording to Marie et al., the bands around 1496 and 1489 cm^{-1} can be attributed to 1,2,4-trimethylbenzene (1,2,4-TMB) and toluene, respectively.[33] A band at 1486 cm^{-1} is observed for sample P and is thus assigned to toluene. The other bands corresponding to this molecule are observed at 1582, 1446, and 1386 cm^{-1}. The 1486 cm^{-1} band is also observed in the spectra of H and HW, as well as the other band characteristic of toluene. In addition, bands at 1602, 1495, 1455, and 1394 cm^{-1} are also observed, especially for sample HW; this could correspond to 1,2,4-TMB. An additional band, at 1536 cm^{-1} does not correspond to either toluene, TMB, or xylene isomers adsorbed at 623 K.

During the first 40 min of N_2 flushing, a 2D-correlation analysis of sample HW (Figure 11) shows that the major changes occurring in the aromatic region are those of toluene (1582, 1486, 1448, and 1385 cm^{-1}) and TMB (1602 cm^{-1}). In the OH region, the silanols at 3740 and 3730 cm^{-1} are mainly affected and negatively correlated to the aromatics desorbed. A small negative correlation peak at {3600, 1602} cm^{-1} indicates also that some Brønsted sites are freed at the onset of desorption. Sample H shows a similar 2D-correlation map. The 2D-correlation map of sample HW flushed in N_2 for 3 h shows a relatively strong evolution of the 1536 cm^{-1} band, as already noticeable in the 1D spectrum (Figure 10). Interestingly, there is no detectable correlation between this band and the silanol groups. One possible interpretation for the 1540 cm^{-1} band is that it corresponds to aromatic molecules adsorbed on Lewis sites located at the external surface. These aromatic molecules are apparently easier to remove from HW than from H; this could be related to the presence of weaker Lewis sites (as shown by IR of absorbed CO, Figure SI3 in the Supporting Information) covered with coke molecules quite easy to remove. Finally, the 1355 cm^{-1} band is not affected by the N_2 flush and hence likely corresponds to "heavy" coke not easily desorbed.

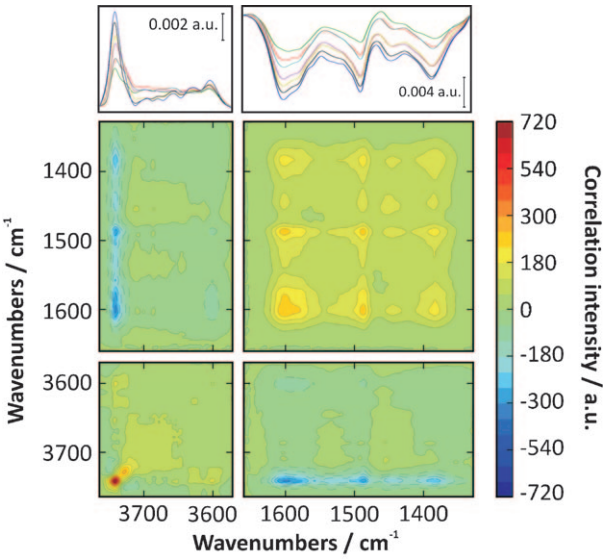

Figure 11. 2D-correlation IR spectra of the sample HW showing the evolution of the band intensity during the first 40 min under pure N_2 flow. The color bars show the correlation intensity scale (i.e., the standard deviation of the whole evolution, multiplied by 10^5). Negative correlation peaks (blue) mean that the two correlated frequencies evolve in opposite directions, whereas positive correlation peaks (red) mean that they evolve in the same direction.

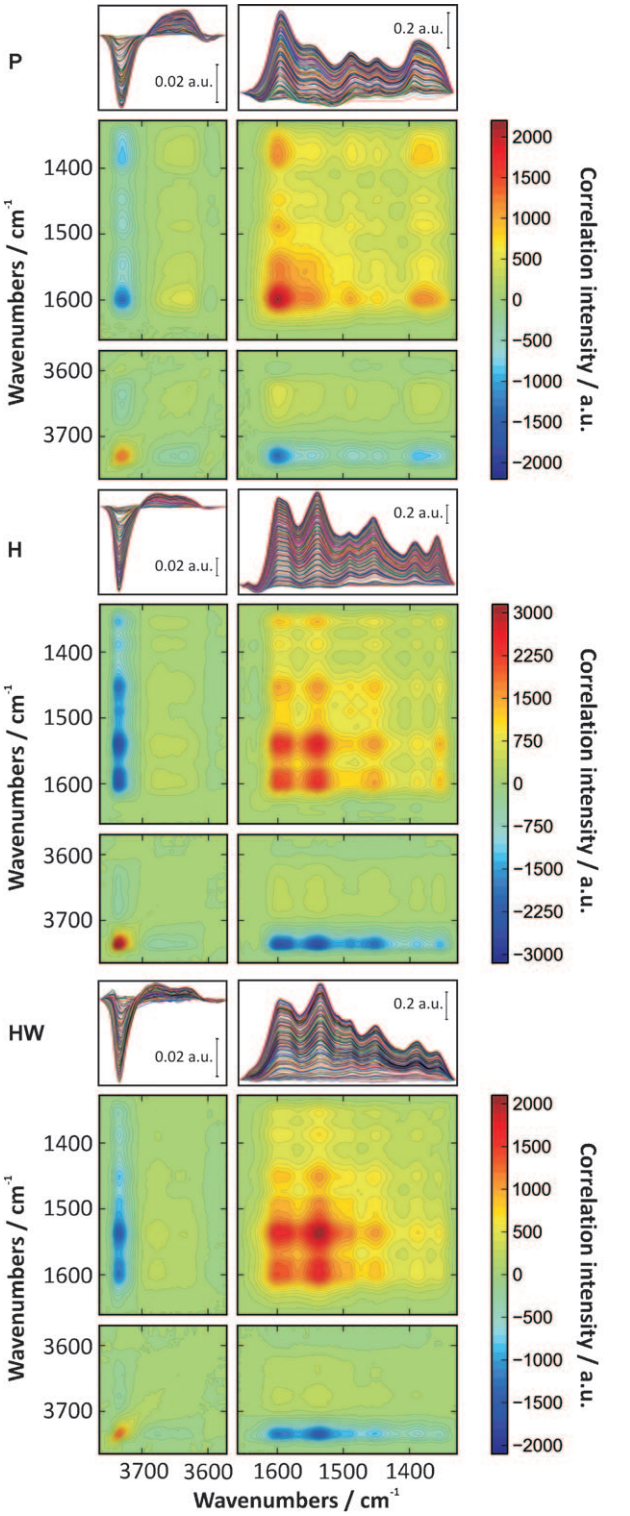

Figure 12. 2D-correlation map of the parent P (top), hierarchical H (middle) and HCl-washed HW (bottom) catalysts showing the correlation between the evolution of the OH and "aromatic" bands during the 17 h of *o*-xylene reaction at 623 K.

Most of the bands appearing in the C–H and C=C regions (Figure 9) are therefore related to heavier aromatics (i.e., coke) that cannot be desorbed at 623 K. The 2D-correlation maps of all the spectra acquired every 6 min during the 17 h of *o*-xylene reaction for the three samples are represented in Figure 12. They capture the entire evolution of the various bands during the catalytic test; the strongest correlations are represented by the denser contours. For all samples, the stronger negative correlations (Figure 12, in blue) between the aromatic and the OH regions are found for the OH band between 3730 and 3740 cm^{-1}, highlighting that the coke is mainly interacting with silanols located at the external surface of the catalyst. A closer look at the {aromatic–aromatic} and {aromatic–OH} correlations indicates that the bands correlating the most (i.e., having the highest cross-peak intensities) are different for the three samples. For the parent zeolite, the strongest cross-peaks are found for the bands at 1601 and 1385–1362 cm^{-1}, whereas for the mesoporous zeolites, the maxima are between 1500 and 1600 cm^{-1}, likely due to a more aromatic character of the coke formed at their external surface. A detailed analysis of these bands and their attribution is quite intricate, as it requires adsorptions of a whole set of aromatic molecules on non-acidic forms of all samples to avoid any catalytic transformation.[33] Further work in this direction is planned, together with a detailed analysis of the hydrocarbons extracted from the used catalysts following the well-established approach of Guisnet et al.[34]

Conclusion

Hierarchical (mesoporous) ZSM-5 zeolites display much improved catalytic performances compared to their purely microporous counterpart in the shape-selective *o*-xylene isomerization, that is, a twofold higher *p*-xylene yield is achieved. An optimum between high catalytic activity (typically found in purely microporous small crystals) and improved selectivity (typically found in purely microporous large crystals) can be engineered with hierarchical porous zeolites. The introduction of intracrystalline mesoporosity by desilication increases the *o*-xylene conversion but decreases *p*-xylene selectivity and catalyst stability due to coke deactivation. The extraction of framework silicon in alkaline medium generates extensive mesoporosity, but also induces substantial changes in acidity by redistribution of some aluminum in the sample. The resulting high concentration of Lewis sites at the external surface and high concentration of Brønsted centers at the pore mouths has a negative influence on the catalyst stability. A consecutive mild HCl treatment of the hierarchical zeolite selectively eliminates these sites, resulting in an increased *p*-xylene selectivity and reduced deactivation rate. Operando IR spectroscopy and 2D-correlation analysis make precise monitoring of the catalytic changes induced by these successive treatments possible and this leads to the design of better catalysts. Our results emphasize the point that knowledge of the nature of the aluminum in mesoporous zeolites is of greater importance than that of purely microporous zeolites, as it may strongly influence the performance of acid-catalyzed (Brønsted or Lewis) reactions. The presence of Lewis sites and their location can be beneficial or detrimental, depending on the specific requirements of the catalytic process under investigation. Hierarchical zeolites present new opportunities and challenges in heterogeneous catalysis. A full utilization of their potential requires a thorough description and understanding of their surface chemistry and its relation to catalytic transformation.

Experimental Section

Materials and treatments: Commercial ZSM-5 zeolite from Zeolyst International (CBV 8014 lot no. 2200–44, nominal Si/Al = 40, NH_4-form) was used as the starting material. The parent sample (denoted P) resulted from calcination of the as-received powder in static air at 823 K for 5 h by using a heating rate of 5 K min^{-1}. These conditions were identical in subsequent calcinations. The alkaline treatment was carried out in a 250 cm^3 round-baker adapted to a reflux-condenser filled with 181 cm^3 of aqueous 0.2 M NaOH and heated at 338 K. The zeolite sample (6 g) was added and stirred magnetically at 500 rpm for 30 min. The suspension was quenched in an ice–water mixture and filtered. The resulting solid was washed, dried at 373 K for 12 h, and calcined. The alkaline-treated sample was brought into the H-form by three successive ion exchanges in a 0.1 M NH_4NO_3 aqueous solution followed by calcination (sample H). Successive acid washing was carried out in a 20 cm^3 glass tube filled with 17 cm^3 of aqueous 0.1 M HCl and heated at 343 K. The zeolite sample (0.55 g) was added and stirred magnetically at 500 rpm for 6 h. The solid was filtered, washed, dried, and calcined (sample HW).

Characterization: Si and Al concentrations in the solids and filtrates obtained by alkaline treatment and acid washing were determined by inductively coupled plasma-optical emission spectroscopy (ICP-OES) (Perkin–Elmer Optima 3200RL (radial)). N_2 isotherms at 77 K were measured in a Quantachrome Quadrasorb-SI gas adsorption analyzer. Prior to the measurements, the samples were degassed under vacuum at 573 K for 10 h. The Brunauer–Emmett (BET) method[35] was applied to calculate the total surface area, which is used for comparative purposes. The *t*-plot method was used to discriminate between micro- and mesoporosity.[36] The mesopore size distribution was obtained by the Barrett–Joyner–Halenda (BJHmodel applied to the adsorption branch of the isotherm.[37] High-resolution low-pressure argon isotherms at 87 K were measured in a Micrometrics ASAP2010 gas adsorption analyzer. Prior to the measurement, the samples were degassed in situ under vacuum at 623 K for 16 h. Transmission electron microscopy (TEM) was carried out in a JEOL JEM 1011 microscope operated at 100 kV. Powder X-ray diffraction (XRD) patterns were measured in a Siemens D5000 diffractometer with Bragg–Brentano geometry and Ni-filtered $Cu_{K\alpha}$ radiation (λ = 0.1541 nm). Data were recorded in the 2θ range 5–50° with an angular step size of 0.05° and a counting time of 8 s per step. The ^{27}Al MAS NMR spectra were recorded at 9.4 T on a Bruker Avance spectrometer with a 4 mm double-bearing MAS probe head, a spinning speed of 14.5 kHz, and a recycling delay of 0.5 s. The radio-frequency (RF) field was 10 kHz and the pulse length was 2 μs (π/12 pulse flip-angle). Infrared spectra were recorded on a Nicolet Magna 550 FTIR spectrometer at 2 cm^{-1} optical resolution, with one level of zero-filling for the Fourier transform. Prior to the measurements, the zeolites were pressed in self-supporting discs (diameter: 1.6 cm, 7 mg cm^{-2}) and were pretreated in the IR cell attached to a vacuum line at 723 K for 4 h up to 10^{-6} Torr. The adsorptions of pyridine, lutidine, and collidine were performed at 300 K in successive doses of 0.3–1 μmol. At the end of each adsorption experiment, a pressure of 1 Torr was established in the cell to reach saturation followed by evacuation at 473 K to remove physically adsorbed species. All spectra were normalized to 10 mg wafers. Difference spectra were ob-

tained by subtracting the spectrum of the zeolite before pyridine adsorption. The amount of adsorbed probe molecule was determined by using the integrated area of bands typical of the protonated (Brønsted) or coordinated (Lewis) forms. The molar absorption coefficients given by Nesterenko et al.[38] were used for pyridine and collidine, and those given by Onfroy et al.[39] for lutidine. Errors in the Brønsted and Lewis quantification are estimated to be approximately 10%: 3–5% for the molar adsorption coefficient, 5% for the integrated area (absorbance), and 1% for mass measurement of the wafer. The strength of the acid sites was evaluated by adsorption of CO at 77 K in the FTIR cell. At this temperature, the interaction between CO and OH groups induce a low frequency shift of OH stretching vibrations and a high frequency shift of the interacting CO vibration bands. These shifts allow the estimation of the strength of the acid sites.[40] X-ray photoelectron spectroscopy (XPS) was measured on a Thermo Scientific K-Alpha ESCA instrument using monochromatic $Al_{K\alpha}$ radiation ($h\nu = 1486.6$ eV) as the X-ray source. Neutralization of the surface charge in the non-conducting samples was performed by using both a low-energy electron flood gun and a low-energy argon ion gun. The surface elemental composition was determined by using the standard Scofield photoemission cross sections. Thermogravimetric analysis (TGA) was carried out in a Mettler Toledo TGA/SDTA851e microbalance. The sample was dried under air flow (70 $cm^3 min^{-1}$) at 373 K for 1 h and then the temperature was ramped from 373 to 1173 K at 5 $K min^{-1}$.

Operando infrared spectroscopy: Catalytic tests were performed in a micro infrared reactor cell already described elsewhere,[41] in which the spectra of both the self-supported catalyst wafer and the adsorbed species were recorded during the reaction, up to a temperature of 623 K. A nitrogen gas stream was diverted to a saturator filled with *o*-xylene maintained at 300 K and the resulting mixture fed the IR reactor cell. Reaction conditions were the following: $T = 623$ K, $p_{o\text{-xylene}} = 4.3$ Torr, and WHSV = 4.1–4.9 h^{-1}. The reaction products exiting the reactor were analyzed by online gas chromatography (Varian GC CP-3800). The IR spectrometer was a Nicolet Magna 750, the number of scans accumulated was set to 128 with at 2 cm^{-1} resolution (Happ–Genzel apodization function), and fitted with an MCT detector. Self-supported pressed discs of the zeolites (diameter 1.6 cm, ≈ 7 mg cm^{-2}) were activated under nitrogen flow (IR cell reactor) up to 673 K by using a heating ramp of 1 $K min^{-1}$. The 2D correlation data treatment method, initially introduced by Noda et al.,[42] was already used successfully in the treatment of operando IR data, and more details can be found in the corresponding papers.[23,43] In this work, the 2D matrix of statistical covariance, C, was first computed for a series of N IR spectra $A(\tilde{\nu},t)$ in the time interval $t = \{t_i, t_f\}$, where $\tilde{\nu}$ are the IR wavenumbers [Eq. (1)]:

$$C(\overline{\nu}_a, \overline{\nu}_b) = \frac{1}{N} \sum_{t=t_i}^{t_f} A(\overline{\nu}_a, t) A(\overline{\nu}_b, t) \quad (1)$$

Then the correlation (or cross-correlation) matrix F is obtained by the following [Eq. (2)]:

$$F(\overline{\nu}_a, \overline{\nu}_b) = \sqrt{C(\overline{\nu}_a, \overline{\nu}_b)} \quad (2)$$

Acknowledgements

This work was supported by the Région Basse-Normandie, the Spanish MICINN (CTQ2006-01562/PPQ, CTQ2009-09824/PPQ, and the Consolider-Ingenio 2010 Grant CSD2006-0003), and the ICIQ Foundation. I.S. is grateful to the French Research Ministry (MESR) for a Ph.D. fellowship. C. Serra (Universidad de Vigo) is acknowledged for XPS analyses. Dr. S. Abelló (ICIQ), Dr. G. Clet, Dr. O. Marie, Dr. F. Maugé, Dr. F. Thibault-Starzyk, and Dr. A. Vimont (LCS-ENSICAEN) are acknowledged for stimulating discussions.

[1] W. Vermeiren, J.-P. Gilson, *Top. Catal.* **2009**, *52*, 1131–1161.
[2] N. Y. Chen, T. F. Degnan, C. Morris Smith, *Molecular Transport and Reaction in Zeolites*, VCH, Weinheim, **1994**; W. O. Haag, N. Y. Chen in *Catalyst Design—Progress and Perspectives* (Eds.: L. L. Hegedus, A. T. Bell, N. Y. Chen, W. O. Haag, J. Wei, R. Aris, M. Boudart, B. C. Gates, G. A. Somorjai), Wiley-Interscience, New York, **1988**, pp. 163–212.
[3] C. Baerlocher, L. B. McCusker, D. H. Olson, *Atlas of Zeolite Framework Types*, Elsevier, Amsterdam, **2007**.
[4] T. F. Degnan, *J. Catal.* **2003**, *216*, 32–46; K. Beschmann, L. Riekert, U. Müller, *J. Catal.* **1994**, *145*, 243–245; J.-H. Kim, T. Kunieda, M. Niwa, *J. Catal.* **1998**, *173*, 433–439.
[5] J. Pérez-Ramírez, C. H. Christensen, K. Egeblad, C. H. Christensen, J. C. Groen, *Chem. Soc. Rev.* **2008**, *37*, 2530–2542.
[6] Y. Li, S. Liu, Z. Zhang, S. Xie, X. Zhu, L. Xu, *Appl. Catal. A* **2008**, *338*, 100.
[7] R. Srivastava, M. Choi, R. Ryoo, *Chem. Commun.* **2006**, 4489–4491.
[8] M. H. F. Kox, E. Stavitski, J. C. Groen, J. Pérez-Ramírez, F. Kapteijn, B. M. Weckhuysen, *Chem. Eur. J.* **2008**, *14*, 1718–1725.
[9] J. Pérez-Ramírez, D. Verboekend, A. Bonilla, S. Abelló, *Adv. Funct. Mater.* **2009**, *19*, 3972–3979; Z. Musilová-Pavlačková, S. Zones, J. Čejka, *Top. Catal.* **2010**, DOI: 10.1007s11244-11009-19410-11242.
[10] D. P. Serrano, R. A. García, D. Otero, *Appl. Catal. A* **2009**, *359*, 69–78.
[11] J. Pérez-Ramírez, S. Abelló, A. Bonilla, J. C. Groen, *Adv. Funct. Mater.* **2009**, *19*, 164–172.
[12] M. Bjørgen, F. Joensen, M. S. Holm, U. Olsbye, K.-P. Lillerud, S. Svelle, *Appl. Catal. A* **2008**, *345*, 43–50.
[13] S. Gopalakrishnan, A. Zampieri, W. Schwieger, *J. Catal.* **2008**, *260*, 193–197.
[14] J. C. Groen, J. A. Moulijn, J. Pérez-Ramírez, *J. Mater. Chem.* **2006**, *16*, 2121–2131.
[15] J.-P. Gilson, E. G. Derouane, *J. Catal.* **1984**, *88*, 538–541; M. Farcasiu, T. F. Degnan, *Ind. Eng. Chem. Res.* **1988**, *27*, 45–47; J. Weitkamp, S. Ernst, L. Puppe in *Catalysis and Zeolites* (Eds.: J. Weitkamp, L. Puppe), Springer, Berlin, **1999**, pp. 336–340.
[16] S. van Donk, A. H. Janssen, J. H. Bitter, K. P. de Jong, *Catal. Rev. Sci. Eng.* **2003**, *45*, 297–319.
[17] V. N. Shetti, J. Kim, R. Srivastava, M. Choiand, R. Ryoo, *J. Catal.* **2008**, *254*, 296–303.
[18] J. C. Groen, J. A. Moulijn, J. Pérez-Ramírez, *Microporous Mesoporous Mater.* **2005**, *87*, 153–161.
[19] Y. N. Li, S. L. Liu, S. J. Xie, L. Y. Xu, *React. Kinet. Catal. Lett.* **2009**, *98*, 117–124; Y. N. Li, S. L. Liu, Z. K. Zhang, S. J. Me, X. X. Zhu, L. Y. Xu, *Appl. Catal. A* **2008**, *338*, 100–113.
[20] N. Malicki, G. Mali, A.-A. Quoineaud, P. Bourges, L. J. Simon, F. Thibault-Starzyk, C. Fernandez, *Microporous Mesoporous Mater.* **2010**, *129*, 100–105.
[21] M. Guisnet, N. S. Gnep, S. Morin, *Microporous Mesoporous Mater.* **2000**, *35–36*, 47–59; J. A. Martens, J. Perez-Pariente, E. Sastre, A. Corma, P. A. Jacobs, *Appl. Catal.* **1988**, *45*, 85–101.
[22] D. H. Olson, G. T. Kerr, S. L. Lawton, W. M. Meier, *J. Phys. Chem.* **1981**, *85*, 2238–2243; D. H. Olson, W. O. Haag in *Catalytic Materials: Relationship Between Structure and Reactivity* (Eds.: T. E. Whyte, R. A. Dalla Betta, E. G. Derouan, R. T. K. Baker), ACS, Washington, **1984**, pp. 275–307.
[23] F. Thibault-Starzyk, A. Vimont, J.-P. Gilson, *Catal. Today* **2001**, *70*, 227–241.
[24] F. Thibault-Starzyk, I. Stan, S. Abelló, A. Bonilla, K. Thomas, C. Fernandez, J.-P. Gilson, J. Pérez-Ramírez, *J. Catal.* **2009**, *264*, 11–14.
[25] J. C. Groen, L. A. A. Peffer, J. A. Moulijn, J. Pérez-Ramírez, *Colloids Surf. A* **2004**, *241*, 53–58.
[26] J. C. Groen, L. A. A. Peffer, J. A. Moulijn, J. Pérez-Ramírez, *Chem. Eur. J.* **2005**, *11*, 4983–4994.
[27] M. S. Holm, S. Svelle, F. Joensen, P. Beato, C. H. Christensen, S. Bordiga, M. Bjørgen, *Appl. Catal. A* **2009**, *356*, 23–30.
[28] J. C. Groen, G. M. Hamminga, J. A. Moulijn, J. Pérez-Ramírez, *Phys. Chem. Chem. Phys.* **2007**, *9*, 4822–4830.
[29] G. Lietz, K. H. Schnabel, C. Peuker, T. Gross, W. Storek, J. Völter, *J. Catal.* **1994**, *148*, 562–568.

[30] M. Paciga, A. Smišková, P. Hudec, V. Židek, *React. Kinet. Catal. Lett.* **1997**, *60*, 21–26; D. Fraenkel, *Ind. Eng. Chem. Res.* **1990**, *29*, 1814–1821.
[31] H. S. Cerqueira, P. Ayrault, J. Datka, M. Guisnet, *Microporous Mesoporous Mater.* **2000**, *38*, 197–205.
[32] A. Vimont, O. Marie, J.-P. Gilson, J. Saussey, F. Thibault-Starzyk, J. C. Lavalley, *Stud. Surf. Sci. Catal.* **1999**, *126*, 147–154; C. L. Li, O. Novaro, E. Munoz, J. L. Boldu, X. Bokimi, J. A. Wang, T. Lopez, R. Gomez, *Appl. Catal. A* **2000**, *199*, 211–220.
[33] O. Marie, F. Thibault-Starzyk, P. Massiani, *J. Catal.* **2005**, *230*, 28–37.
[34] M. Guisnet, L. Costaa, F. Ribeiro, *J. Mol. Catal. A* **2009**, *305*, 69–83.
[35] S. Brunauer, P. H. Emmett, E. Teller, *J. Am. Chem. Soc.* **1938**, *60*, 309–319.
[36] B. C. Lippens, J. H. de Boer, *J. Catal.* **1965**, *4*, 319–323.
[37] E. P. Barrett, L. G. Joyner, P. H. Hallenda, *J. Am. Chem. Soc.* **1951**, *73*, 373–380.
[38] N. S. Nesterenko, F. Thibault-Starzyk, V. Montouillout, V. V. Yuschenko, C. Fernandez, J.-P. Gilson, F. Fajula, I. I. Ivanova, *Microporous Mesoporous Mater.* **2004**, *71*, 157–166.
[39] T. Onfroy, G. Clet, M. Houalla, *Microporous Mesoporous Mater.* **2005**, *82*, 99–104.
[40] O. Cairon, T. Chevreau, J. C. Lavalley, *J. Chem. Soc. Faraday Trans.* **1998**, *94*, 3039–3047.
[41] T. Lesage, C. Verrier, P. Bazin, J. Saussey, M. Daturi, *Phys. Chem. Chem. Phys.* **2003**, *5*, 4435–4440.
[42] I. Noda, A. E. Dowrey, C. Marcott, *Mikrochim. Acta* **1988**, 101–103; I. Noda, *Appl. Spectrosc.* **1993**, *47*, 1329–1336.
[43] F. Thibault-Starzyk, A. Vimont, C. Fernandez, J. P. Gilson, *Chem. Commun.* **2000**, 1003–1004.

Received: December 14, 2009
Published online: April 15, 2010

